ACS APPLIED MATERIALS & INTERFACES

Research Article

Cite This: ACS Appl. Mater. Interfaces 2018, 10, 1125−1131

www.acsami.org

Carrier Trapping by Oxygen Impurities in Molybdenum Diselenide

Ke Chen,[†] Anupam Roy,[‡] Amritesh Rai,[‡] Amithraj Valsaraj,[‡] Xianghai Meng,[†] Feng He,[†,∥] Xiaochuan Xu,[§] Leonard F. Register,[‡] Sanjay Banerjee,[‡] and Yaguo Wang*[,†,∥]

[†] Department of Mechanical Engineering and [∥] Texas Materials Institute, The University of Texas at Austin, Austin, Texas 78712, United States

[‡] Microelectronics Research Center and Department of Electrical and Computer Engineering, The University of Texas at Austin, Austin, Texas 78758, United States

[§] Omega Optics, Inc., Austin, Texas 78757, United States

Supporting Information

ABSTRACT: Understanding defect effect on carrier dynamics is essential for both fundamental physics and potential applications of transition metal dichalcogenides (TMDs). Here, the phenomenon of oxygen impurities trapping photoexcited carriers has been studied with ultrafast pump-probe spectroscopy. Oxygen impurities are intentionally created in exfoliated multilayer $MoSe_2$ with Ar^+ plasma irradiation and air exposure. After plasma treatment, the signal of transient absorption first increases and then decreases, which is a signature of defect-capturing carriers. With larger density of oxygen defects, the trapping effect becomes more prominent. The trapping defect densities are estimated from the transient absorption signal, and its increasing trend in the longer-irradiated sample agrees with the results from X-ray photoelectron spectroscopy. First-principle calculations with density functional theory reveal that oxygen atoms occupying Mo vacancies create mid-gap defect states, which are responsible for carrier trapping. Our findings shed light on the important role of oxygen defects as carrier trappers in TMDs, and facilitate defect engineering in relevant materials and device applications.

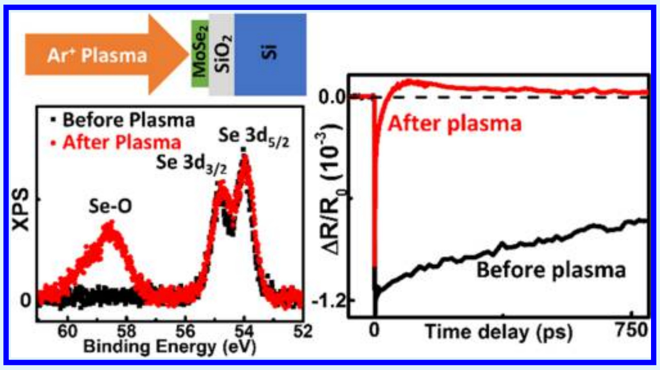

KEYWORDS: *carrier trapping, defect, oxygen impurity,* $MoSe_2$

1. INTRODUCTION

In the past few years, layered materials transition metal dichalcogenides (TMDs) have attracted numerous research interests because of their extraordinary properties, such as direct band gap in monolayer samples,[1] stable excitons and trions at room temperature,[2] superior immunity to short channel effects,[3] and strong spin−valley coupling,[4] which make TMDs promising for applications in nano- and flexible electronics, photonics, and valleytronics. For many of these TMD-based devices, it is essential to understand the physics of carrier-related interactions[5] and to acquire carrier transport properties that determine the key performance metrics (e.g., bandwidth and responsivity), such as carrier lifetime,[6] diffusion coefficient,[7] and mobility.[8]

Defects inside TMDs or from their environments (substrates and surface adsorbates) can interact with excitons/carriers and significantly affect the functionalities of the electronic devices. For example, the chalcogen vacancy defect[9] and its related complex[10] are able to activate additional defect-associated photoluminescence (PL) channels, which can decrease the intrinsic exciton PL efficiency. Charged impurity scattering due to either the ionized impurities inside TMDs[11] or charge traps at the surface of the substrate[12] has been proposed to be the dominant factor for the observed low room-temperature mobility in TMD devices. Charge traps at the TMD-gate insulator interface have also been suggested as the cause of hysteresis in TMD-based field-effect transistors.[13] Some defects can also serve as recombination centers, assisting the recombination of the photoexcited excitons/carriers in exfoliated few-layer and multilayer TMDs via Auger scattering.[14,15]

Even though the defect-trapping effect from oxygen impurities was proposed to be responsible for the previously observed phenomena in chemical vapor deposition (CVD)-grown monolayer and multilayer $MoSe_2$,[16] direct evidence and mechanisms about how these impurities are introduced into the samples, and more importantly, their effects on the electronic band structure and carrier dynamics are still not fully understood. In this paper, we intentionally created oxygen defects in exfoliated multilayer $MoSe_2$ by plasma irradiation and then studied and verified the effect of the generated oxygen defects on the photoexcited carrier dynamics with femtosecond

Received: October 13, 2017
Accepted: December 11, 2017
Published: December 11, 2017

DOI: 10.1021/acsami.7b15478

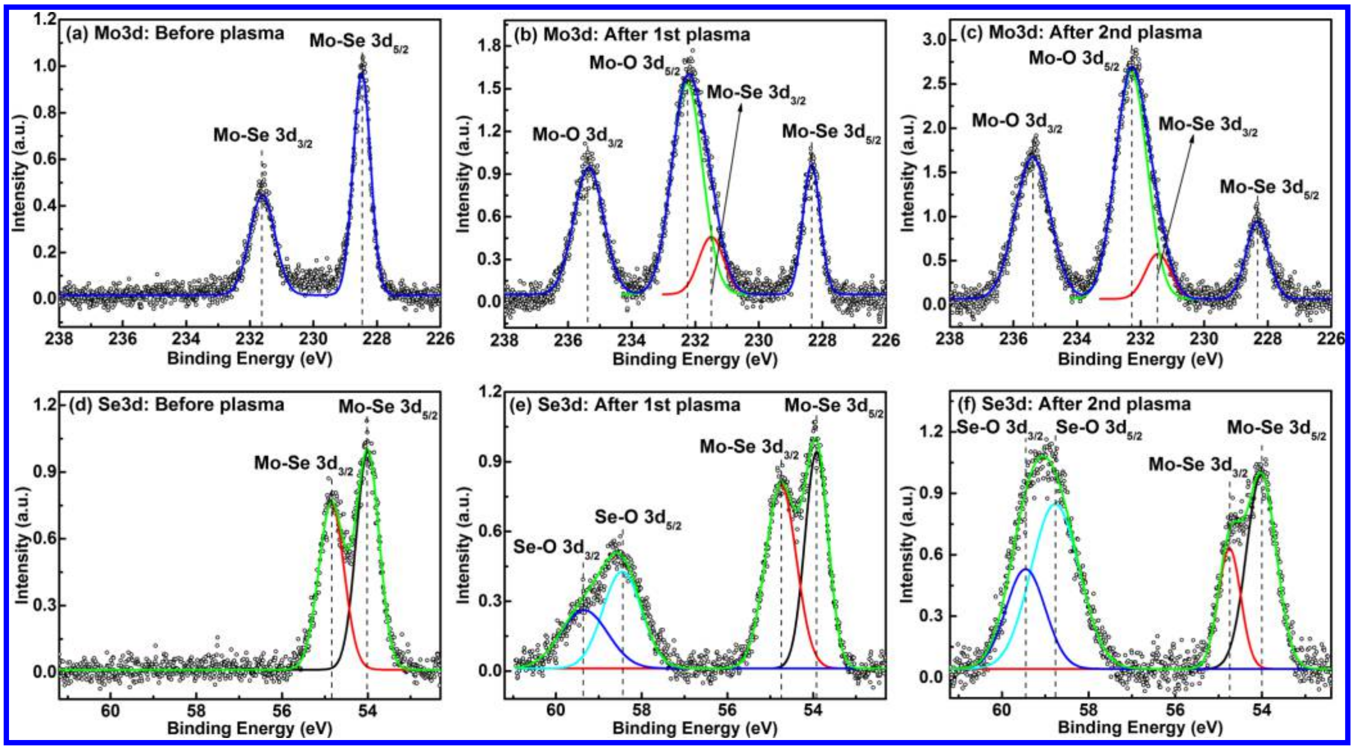

Figure 1. XPS data of the $MoSe_2$ sample before plasma irradiation (a,d), after the first plasma irradiation (b,e), and after the second plasma irradiation (c,f). Peaks of Mo−O and Se−O bonds can be clearly seen after plasma irradiation, and the relative intensities of these oxygen bonding peaks increase after the second plasma treatment.

laser pump-probe spectroscopy. The optical signature of carriers being trapped by mid-gap defects is observed after plasma irradiation, and the defect-capturing-carrier effect increases with oxygen defect density. Our experimental findings, along with a band structure calculation with density functional theory (DFT), confirm the carrier-trapping role of oxygen impurities in $MoSe_2$ and provide important implications for defect engineering in TMD-based devices.

2. RESULTS AND DISCUSSION

2.1. Ar^+ Plasma Irradiation and XPS Characterization . Multilayer $MoSe_2$ samples were mechanically exfoliated from the commercial $MoSe_2$ crystal (two-dimensional semiconductors) onto a SiO_2/Si substrate using a scotch tape. Because it has been found that the defect-trapping exciton/carrier phenomenon occurs regardless of the sample thickness,[16] indicating that the sample thickness is not a crucial factor, a relatively thick flake [80 nm thickness confirmed by atomic force microscopy (AFM), see Supporting Information] with lateral dimensions >20 μm was chosen to provide large enough sample area for our laser spot (20 μm in diameter).

Plasma irradiation is an effective means to generate defects in TMD materials[17] or to reduce the thickness of layered materials.[18] It has been demonstrated that oxygen impurity can be created in MoS_2 samples after Ar^+ plasma treatment.[19] Initially, the Ar^+ plasma generates vacancies and new edge defects, and then the vacancies and the new edges will be occupied or oxidized by oxygen atoms once exposed to air. Following this method, we performed two sequential Ar^+ plasma irradiations on our $MoSe_2$ sample using a reactive ion etcher (Plasma-Therm 790 RIE). The recipe used in the plasma treatment is 50 W power, 200 mTorr pressure, 20 sccm Ar flow rate but with 30 s irradiation time for the first treatment and 300 s for the second treatment. To verify the generation of defects, as well as to identify the defect species, we measured the samples with X-ray photoelectron spectroscopy (XPS) after each plasma treatment, as shown in Figure 1. Before plasma irradiation, Mo $3d_{5/2}$ and Mo $3d_{3/2}$ peaks, located at 228.5 and 231.6 eV, respectively, and Se $3d_{5/2}$ and Se $3d_{3/2}$ peaks, located at 54 and 54.8 eV, respectively, can be observed. These peak positions agree with the reference values of Mo−Se bonding.[20,21] After the first plasma treatment (30 s), four new peaks appear, located at around 232.3, 235.4, 58.6, and 59.4 eV. Comparing with the literature results,[22,23] two of these peaks originate from the electrons in the Mo 3d shell with $j = 5/2$ and $j = 3/2$ in Mo−O bonds and the other two peaks from the electrons in the Se 3d shell with $j = 5/2$ and $j = 3/2$ in Se−O bonds, respectively. The observation of these peaks indicates that we have successfully created oxygen impurities with chemical bonds to both Mo and Se atoms in the material. After the second plasma treatment, for which the irradiation time is 10 times of the first treatment, the relative intensities of the Mo−Se bonding peaks decrease, whereas those of the Mo−O and Se−O bonding peaks increase. This indicates that more Mo−Se bonds were destroyed and more oxide bonds were created, that is, the density of oxygen impurities increases, with the longer irradiation time.

2.2. Differential Reflection in Pristine Exfoliated $MoSe_2$. The controllable generation of oxygen impurities allows us to investigate their effect on carrier dynamics by directly comparing the differential reflection signals before and after plasma treatments. We measured the differential reflection, $\Delta R/R_0 = (R - R_0)/R_0$, with femtosecond laser pump-probe spectroscopy, where R_0 and R are the reflections of probe pulse before and after excitation by the pump pulse, respectively. The laser pulses are generated from a Ti:sapphire femtosecond laser oscillator, with about 100 fs pulse width, 800 nm central wavelength, and 80 MHz repetition rate. Figure 2a shows the obtained $\Delta R/R_0$ signals at different pump fluences before plasma treatment. All of the signals show negative exponential decays. Figure 2b illustrates the carrier generation and relaxation dynamics in bulk $MoSe_2$.[24] Because the energy difference between the conduction-band minimum and the valence-band maximum at the K point is around 1.51 eV, we can generate and detect electrons and holes in the K valleys nearly resonantly with 800 nm pump and probe pulses, respectively. When probing resonantly, the reflection change is mainly due to the change in absorption caused by the phase-space-filling effect.[25] Details about the relation between the differential reflection and the refractive index change can be found in the Supporting Information. The optical penetration depth of our laser in the $MoSe_2$ material is about 55 nm,[26] comparable to the sample thickness. In this case, the reflection of the multilayer $MoSe_2/SiO_2/Si$ structure needs to be calculated by the transfer matrix method, and the derived expression is[27]

$$R = \left| \frac{r_1\, e^{i(\varphi_1+\varphi_2)} + r_2\, e^{-i(\varphi_1-\varphi_2)} + r_3\, e^{-i(\varphi_1+\varphi_2)} + r_1 r_2 r_3\, e^{-i(\varphi_1-\varphi_2)}}{e^{i(\varphi_1+\varphi_2)} + r_1 r_2\, e^{-i(\varphi_1-\varphi_2)} + r_1 r_3\, e^{-i(\varphi_1+\varphi_2)} + r_2 r_3\, e^{-i(\varphi_1-\varphi_2)}} \right|^2 \tag{1}$$

where $r_1 = \frac{\tilde{n}_0 - \tilde{n}_1}{\tilde{n}_0 + \tilde{n}_1}$, $r_2 = \frac{\tilde{n}_1 - \tilde{n}_2}{\tilde{n}_1 + \tilde{n}_2}$, and $r_3 = \frac{\tilde{n}_2 - \tilde{n}_3}{\tilde{n}_2 + \tilde{n}_3}$ are the complex amplitude of reflection coefficients for air/$MoSe_2$, $MoSe_2/SiO_2$, and SiO_2/Si interfaces, respectively; $\tilde{n}_i = n_i - i\kappa_i$ is the complex refractive index of each material (note that positive κ stands for absorption); and $\varphi_i = 2\pi\tilde{n}_i d_i/\lambda$ is the complex phase shift due to a change in the optical path and the absorption in $MoSe_2$ or Si. Using eq 1, the relative reflection change, $\Delta R/R_0$, is plotted as a function of $\Delta\kappa/\kappa$ in the inset of Figure 2a. It can be seen that the reflection change is proportional to the absorption change with a positive slope. Therefore, the observed negative reflection change means that the absorption in the sample decreases after the pump excitation due to the phase-space-filling effect. When the excited carriers occupy the K valleys and reduce the relevant direct transition probability due to Pauli blocking, absorption of the probe becomes less compared with that before pump excitation. In Figure 2a, there are two decay components in the negative reflection change signals, with the fast one only lasting for several picoseconds and the slow one persisting for several hundred picoseconds. The fast decay component can be attributed to carrier redistribution (mainly from the carrier cooling effect) via intravalley and intervalley scatterings, which are accomplished by numerous processes of carrier−carrier scattering and carrier−phonon scattering, as shown in Figure 2b. The slow decay component depicts the recovery of the reduced direct transition probability back to the unexcited level, which reflects the decrease of the excited carrier population in the K valleys, as also shown in Figure 2b.[25] Note that the $\Delta R/R_0$ signal should only be sensitive to the carriers in the K valleys (see Supporting Information for details). The decay rate of the slow component increases with the pump fluences (see the Supporting Information for the normalized $\Delta R/R_0$ signals), indicating that many-body effect (very likely the Auger process)[28,29] is responsible for carrier recombination at high carrier densities.

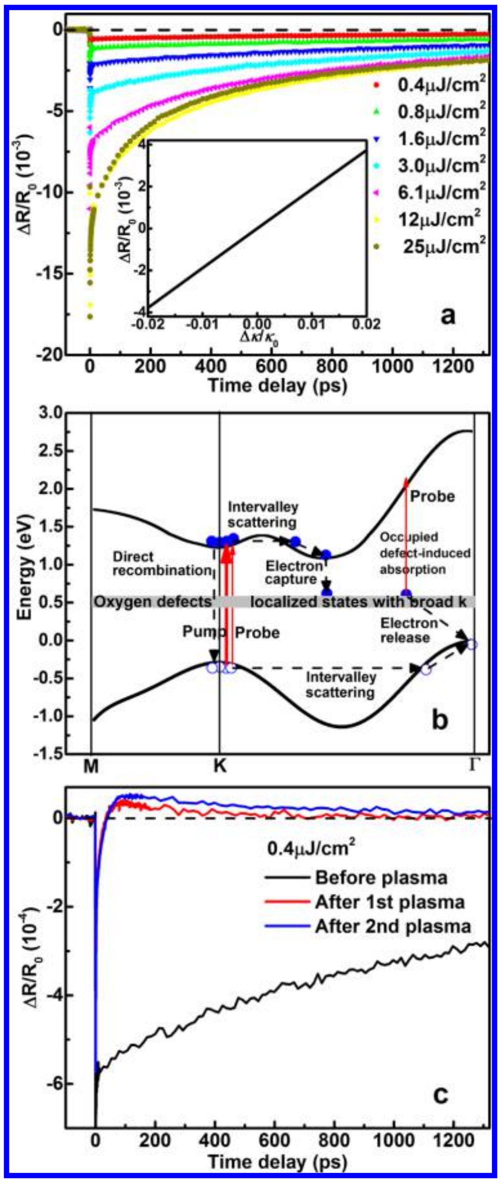

Figure 2. (a) Transient differential reflection signals $\Delta R/R_0$, measured at different pump fluences. (b) Schematic diagram of the photoexcited carrier dynamics in multilayer $MoSe_2$, including carrier generation, intervalley scattering, and carrier trapping by the mid-gap defects. Only electron capture is shown for simplicity. (c) Comparison of $\Delta R/R_0$ before and after plasma treatment at 0.4 $\mu J/cm^2$ pump fluence.

2.3. Comparison of Differential Reflections before and after Plasma Irradiation.

The comparison of $\Delta R/R_0$ signals before and after the first and second plasma treatments is shown in Figure 2c. At low pump fluences, one prominent feature of $\Delta R/R_0$ after plasma irradiation is the sign change of the signals from negative to positive, indicating that the absorption first decreases and then increases. Such an sign-changing transient signal, that indicates of an initial decrease followed by an enhancement in absorption, has been observed in a number of defected materials, such as low temperature-grown (LTG) traditional semiconductors grown with molecular beam epitaxy (LTG-GaAs,[30,31] LTG-InP,[32] and LTG-InGaP[32]) and CVD-grown layered $MoSe_2$ films,[16] and is well-accepted as the signature of defect-capturing-carrier phenomenon. As shown in Figure 2b, when electrons (holes) are just excited into the conduction band (the valence band), the phase-space-filling effect can cause absorption decrease. However, if the material has a considerable amount of mid-gap defects, the excited carriers will be quickly captured and trapped by those mid-gap defects. Once the carriers are captured, an additional absorption channel for the probe, that is, the transition from the localized defect states which possess broad momenta to high energy states in the conduction band (or the valence band for holes), becomes available, leading to an increase in the absorption. In our previous study,[16] we have observed the carrier-trapping phenomena only in CVD-grown $MoSe_2$ films, not in exfoliated flakes. The observed difference between CVD films and the exfoliated flakes comes from the oxygen content that could only be found in CVD samples; hence, oxygen impurities have been proposed to be responsible for carrier-trapping events. Our previous observation also rules out the relevance of Se and Mo vacancies because these vacancies can be found in both exfoliated and CVD-grown TMD materials, with similar density for each vacancy configuration.[33] Here, the fact that the defect-capturing-carrier signature can again be observed after the generation of oxygen impurities in the exfoliated sample by plasma irradiation serves as a strong evidence that oxygen impurities in $MoSe_2$ samples are indeed the effective carrier trappers. While the negatively decaying black curve in Figure 2c shows the recombination of free *K*-valley carriers in the untreated sample, the positively decaying red and blue signals in Figure 2c reflect the process of carrier releasing from the defect states back to the valence band, as shown in Figure 2b.

2.4. Dependence of $\Delta R/R_0$ Signals on the Excited Carrier Density. The $\Delta R/R_0$ signals after the first and second plasma treatments at different pump fluences are shown in Figure 3a,b, respectively. The competition between the trapped carriers and the excess free carriers and the defect saturation effect can be investigated from the pump-fluence-dependent $\Delta R/R_0$ signals. Figure 3a,b shows that the sign-changing signals can only be observed at low pump fluences. As pump power increases, the $\Delta R/R_0$ signals will again become totally negative. This is because when the pump fluence is large enough, the excited carrier density will surpass the defect density, so all of the defects will be occupied, and the effects from excess free carriers will arise. In this case, the final $\Delta R/R_0$ signal is a result of two competing mechanisms: the trapped carriers that contribute positively to the signal via providing additional absorption channels and the excess free carriers that contribute negatively to the signal through the Pauli blocking effect. Obviously when the excited carrier density is much larger than the defect density, the effect from excess free carriers will be dominant and the signal will become totally negative, as shown by the results taken at high fluences in Figure 3a,b. At the highest carrier densities, it can be found that the decay time constants of the later part of the $\Delta R/R_0$ signals in the plasma-treated sample and in the pristine sample are close (see Supporting Information for detail), indicating that the overwhelming excess free carriers recover the system to a condition similar to the pristine case.

2.5. Estimation of the Density of Carrier Trappers. Another interesting feature of the $\Delta R/R_0$ signals is the changing trend of the positive plateau values. As the pump fluence increases, the plateau value first increases then decreases and the value around that time delay finally decreases down to the negative region, as marked by the dashed lines in Figure 3a,b. Using the transfer matrix method, with the reflectance at the $MoSe_2$ surface (R_0) and the transmittance into the Si substrate (T) known, the absorptance within the $MoSe_2$ ($A = 1 - R_0 - T$) can be calculated.[34] With the obtained absorptance and assuming each absorbed photon only generates one electron–hole pair, we convert the pump fluence to the excited carrier density (the validity of this treatment is analyzed in the Supporting Information) and plot the $\Delta R/R_0$ values along the vertical dashed lines as a function of excited carrier density, as shown in Figure 3c. The initially increasing then decreasing trend can be seen very clearly. This trend actually reflects the defect saturation effect: before defect saturation, more excited carriers will result in more occupied defects, and hence a larger positive signal; after defect saturation, more excited carriers will result in more excess free carriers which can compete with the trapped carriers and drag the total signal downward. As a result, more excited carriers will lead to more negative signals once the defects are saturated. Thus, the trend-turning point indicated by the dashed lines in Figure 3c actually corresponds to the density of the available trapping defects in the sample. The estimated defect densities after the first and second plasma

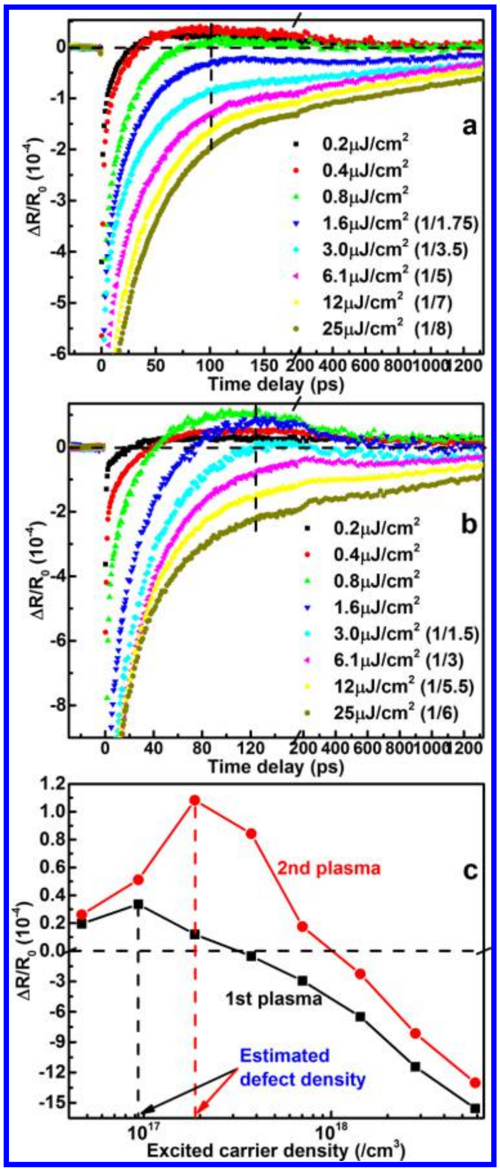

Figure 3. Transient differential reflection signals $\Delta R/R_0$, measured at different pump fluences (a) after the first and (b) after the second plasma irradiation. The signals at high fluences have been scaled with factors for clarity (indicated in the legend). (c) $\Delta R/R_0$ values at time delays marked with dashed lines in a and b, as a function of excited carrier density.

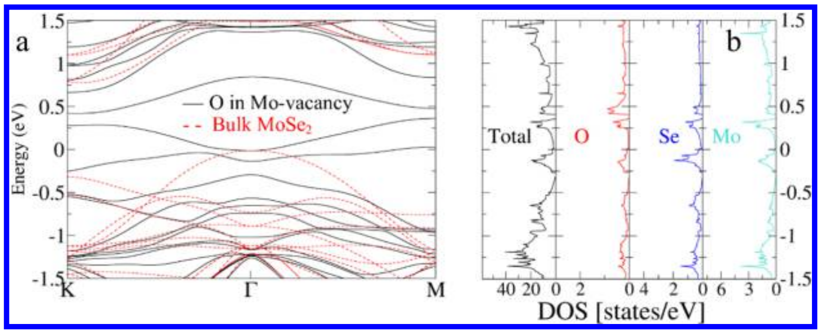

Figure 4. (a) DFT calculation of band structures of bulk $MoSe_2$ without defects and with oxygen atoms sitting in Mo sites. Mid-gap states can be seen clearly when O atoms occupy the Mo vacancies. (b) Atom-projected density of state for $MoSe_2$ with oxygen atoms in Mo vacancy.

treatments are $9.4 \times 10^{16}/\text{cm}^3$ and $1.8 \times 10^{17}/\text{cm}^3$, respectively. These results are consistent with the observation from the XPS data that after the second plasma treatment, the oxygen impurity density increases. In other words, when the oxygen impurity density increases, the trapping defect density estimated from the $\Delta R/R_0$ signal also increases accordingly, which serves as another evidence for the carrier-trapping role of the oxygen impurities.

2.6. DFT Calculation of the Band Structure of $MoSe_2$ with Oxygen Impurities. Finally, we want to discuss about the specific types of oxygen impurities in $MoSe_2$. Although we have demonstrated that oxygen impurities are responsible for carrier trapping, it is still not clear which oxygen bonding is relevant, Mo−O (oxygen atoms occupying Se vacancies) or Se−O (oxygen atoms occupying Mo vacancies) or both? Shallow defects usually serve as donors or acceptors in a material, whereas deep mid-gap defects can serve as carrier trappers or recombination centers.[35] Thus, the key to answer this question is the position of defect state in the band structure, that is, whether the bonding introduces mid-gap state in the band gap. Theoretical calculations with DFT have shown that both molybdenum and chalcogen vacancies can induce mid-gap state within the band gap.[36−40] However, the occupation of the chalcogen vacancy by an oxygen atom (Mo−O bonding) can remove the mid-gap state and restore the band structure to a clean defect-free band gap.[36−38] In oxygen-treated MoS_2 samples, substitution of chalcogen vacancy defects with oxygen atoms (Mo−O bonding) has been shown experimentally to improve the PL efficiency[36] and enhance carrier mobility.[41] Therefore, the question that remains is whether introducing oxygen atoms into the Mo vacancy sites to form Se−O bonding will also passivate the mid-gap states. We have performed DFT calculations to obtain the band structure of bulk $MoSe_2$ with O atoms occupying Mo vacancy sites. Details of DFT calculations can be found in the Supporting Information. As can be seen in Figure 4, after O atoms occupy the Mo vacancy sites, additional defect states that locate deeply inside the original band gap of bulk $MoSe_2$ appear. These mid-gap states can serve as effective carrier trappers (note that recombination center is just a special case of carrier trapper with comparable electron and hole capturing rates).[35] Therefore, considering together the DFT result and our experimental observations, we can conclude that oxygen impurities occupying Mo vacancy sites (and forming Se−O bonding) generate mid-gap defect states and play the role as carrier trapper in the $MoSe_2$ material. Our results imply that even the same defect species, for example, oxygen atoms in this case, can have remarkably different effects on band structure and carrier dynamics in TMDs, depending on their position in the host lattice. When utilizing defect engineering to tune the optical and electrical properties of TMD materials, we need to know not only the defect species but also how these defects interact with the host lattice, as both of these aspects are important to realize the desired functionality.

3. CONCLUSIONS

In summary, we have successfully created oxygen impurities in exfoliated multilayer $MoSe_2$ by Ar^+ plasma irradiation. The generation and increase of oxygen defects after each treatment are confirmed by XPS. Transient reflection signals $\Delta R/R_0$ before plasma treatment are composed of two negative fast and slow decays that reflect the inter-/intra-valley scatterings and recombination of the excited carriers. The $\Delta R/R_0$ signals after plasma treatments exhibit a rapid sign change from negative to positive, a signature of defect trapping carriers, revealing the process of the excited carriers being captured by the created oxygen impurities. The density of oxygen impurities can be estimated from the $\Delta R/R_0$ values of the positive plateau, as a function of the density of excited carrier, and the result of the increased defect density in the longer-irradiated sample agrees with the XPS observation. Moreover, DFT calculations show that oxygen atoms in Mo vacancy sites are responsible for the mid-gap defect states that accounts for carrier trapping. Our findings shed light on the understanding of the interaction between charge carrier and oxygen defect in TMD materials and provide important implications for defect engineering in TMD-based devices.

■ ASSOCIATED CONTENT

Ⓢ Supporting Information

The Supporting Information is available free of charge on the ACS Publications website at DOI: 10.1021/acsami.7b15478.

> Determination of $MoSe_2$ flake thickness with AFM; analysis of the relation between differential reflection and the refractive index change; analysis of the relative importance of direct transition and indirect transition in the signal detection; normalized $\Delta R/R_0$ signals of the pristine $MoSe_2$; comparison between $\Delta R/R_0$ signals of the pristine $MoSe_2$ and the plasma-treated $MoSe_2$ at high carrier densities; estimation of the excited carrier density; and details of DFT calculation for the band structure of $MoSe_2$ with O atoms occupying Mo vacancy sites (PDF)

■ AUTHOR INFORMATION

Corresponding Author

*E-mail: yaguo.wang@austin.utexas.edu.

ORCID

Ke Chen: 0000-0001-7646-8193
Amritesh Rai: 0000-0002-2639-711X
Yaguo Wang: 0000-0002-0448-5645

Notes

The authors declare no competing financial interest.

ACKNOWLEDGMENTS

The authors acknowledge supports from National Science Foundation (NASCENT, grant no. EEC-1160494; CAREER, grant no. CBET-1351881), Department of Energy (SBIR/STTR, grant no. DE-SC0013178), DOD_Army (grant no. W911NF-16-1-0559), and the US Army Research Office (MURI award no. W911NF-17-1-0312). The authors thank Dr. Tiger Hu Tao and Shaoqing Zhang for the AFM measurements.

REFERENCES

(1) Mak, K. F.; Lee, C.; Hone, J.; Shan, J.; Heinz, T. F. Atomically thin MoS_2: a new direct-gap semiconductor. *Phys. Rev. Lett.* **2010**, *105*, 136805.

(2) Mak, K. F.; He, K.; Lee, C.; Lee, G. H.; Hone, J.; Heinz, T. F.; Shan, J. Tightly bound trions in monolayer MoS_2. *Nat. Mater.* **2013**, *12*, 207−211.

(3) Liu, H.; Neal, A. T.; Ye, P. D. Channel length scaling of MoS_2 MOSFETs. *ACS Nano* **2012**, *6*, 8563−8569.

(4) Xu, X.; Yao, W.; Xiao, D.; Heinz, T. F. Spin and pseudospins in layered transition metal dichalcogenides. *Nat. Phys.* **2014**, *10*, 343−350.

(5) Ceballos, F.; Zhao, H. Ultrafast Laser Spectroscopy of Two-Dimensional Materials Beyond Graphene. *Adv. Funct. Mater.* **2017**, *27*, 1604509.

(6) Wang, R.; Ruzicka, B. A.; Kumar, N.; Bellus, M. Z.; Chiu, H.-Y.; Zhao, H. Ultrafast and spatially resolved studies of charge carriers in atomically thin molybdenum disulfide. *Phys. Rev. B: Condens. Matter Mater. Phys.* **2012**, *86*, 045406.

(7) Chen, K.; Yogeesh, M. N.; Huang, Y.; Zhang, S.; He, F.; Meng, X.; Fang, S.; Sheehan, N.; Tao, T. H.; Bank, S. R.; Lin, J.-F.; Akinwande, D.; Sutter, P.; Lai, T.; Wang, Y. Non-destructive measurement of photoexcited carrier transport in graphene with ultrafast grating imaging technique. *Carbon* **2016**, *107*, 233−239.

(8) Strait, J. H.; Nene, P.; Rana, F. High intrinsic mobility and ultrafast carrier dynamics in multilayer metal-dichalcogenide MoS_2. *Phys. Rev. B: Condens. Matter Mater. Phys.* **2014**, *90*, 245402.

(9) Tongay, S.; Suh, J.; Ataca, C.; Fan, W.; Luce, A.; Kang, J. S.; Liu, J.; Ko, C.; Raghunathanan, R.; Zhou, J. Defects activated photoluminescence in two-dimensional semiconductors: interplay between bound, charged and free excitons. *Sci. Rep.* **2013**, *3*, 2657.

(10) Wu, Z.; Luo, Z.; Shen, Y.; Zhao, W.; Wang, W.; Nan, H.; Guo, X.; Sun, L.; Wang, X.; You, Y. Defects as a factor limiting carrier mobility in WSe_2: A spectroscopic investigation. *Nano Res.* **2016**, *9*, 3622−3631.

(11) Ghatak, S.; Pal, A. N.; Ghosh, A. Nature of electronic states in atomically thin MoS_2 field-effect transistors. *ACS Nano* **2011**, *5*, 7707−7712.

(12) Ma, N.; Jena, D. Charge scattering and mobility in atomically thin semiconductors. *Phys. Rev. X* **2014**, *4*, 011043.

(13) Illarionov, Y. Y.; Rzepa, G.; Waltl, M.; Knobloch, T.; Grill, A.; Furchi, M. M.; Mueller, T.; Grasser, T. The role of charge trapping in MoS_2/SiO_2 and MoS_2/hBN field-effect transistors. *2D Mater.* **2016**, *3*, 035004.

(14) Wang, H.; Zhang, C.; Rana, F. Ultrafast dynamics of defect-assisted electron−hole recombination in monolayer MoS_2. *Nano Lett.* **2014**, *15*, 339−345.

(15) Wang, H.; Zhang, C.; Rana, F. Surface recombination limited lifetimes of photoexcited carriers in few-layer transition metal dichalcogenide MoS_2. *Nano Lett.* **2015**, *15*, 8204−8210.

(16) Chen, K.; Ghosh, R.; Meng, X.; Roy, A.; Kim, J.-S.; He, F.; Mason, S. C.; Xu, X.; Lin, J.-F.; Akinwande, D.; Banerjee, S. K.; Wang, Y. Experimental evidence of exciton capture by mid-gap defects in CVD grown monolayer $MoSe_2$. *npj 2D Mater. Appl.* **2017**, *1*, 15.

(17) Chow, P. K.; Jacobs-Gedrim, R. B.; Gao, J.; Lu, T.-M.; Yu, B.; Terrones, H.; Koratkar, N. Defect-induced photoluminescence in monolayer semiconducting transition metal dichalcogenides. *ACS Nano* **2015**, *9*, 1520−1527.

(18) Liu, Y.; Nan, H.; Wu, X.; Pan, W.; Wang, W.; Bai, J.; Zhao, W.; Sun, L.; Wang, X.; Ni, Z. Layer-by-layer thinning of MoS_2 by plasma. *ACS Nano* **2013**, *7*, 4202−4209.

(19) Tao, L.; Duan, X.; Wang, C.; Duan, X.; Wang, S. Plasma-engineered MoS_2 thin-film as an efficient electrocatalyst for hydrogen evolution reaction. *Chem. Commun.* **2015**, *51*, 7470−7473.

(20) Vishwanath, S.; Liu, X.; Rouvimov, S.; Mende, P. C.; Azcatl, A.; McDonnell, S.; Wallace, R. M.; Feenstra, R. M.; Furdyna, J. K.; Jena, D. Comprehensive structural and optical characterization of MBE grown $MoSe_2$ on graphite, CaF_2 and graphene. *2D Mater.* **2015**, *2*, 024007.

(21) Azcatl, A.; Santosh, K. C.; Peng, X.; Lu, N.; McDonnell, S.; Qin, X.; de Dios, F.; Addou, R.; Kim, J.; Kim, M. J. HfO_2 on UV−O_3 exposed transition metal dichalcogenides: interfacial reactions study. *2D Mater.* **2015**, *2*, 014004.

(22) Yao, W.; Iwai, H.; Ye, J. Effects of molybdenum substitution on the photocatalytic behavior of $BiVO_4$. *Dalton Trans.* **2008**, 1426−1430.

(23) Chen, H.-Y.; Su, H.-C.; Chen, C.-H.; Liu, K.-L.; Tsai, C.-M.; Yen, S.-J.; Yew, T.-R. Indium-doped molybdenum oxide as a new p-type transparent conductive oxide. *J. Mater. Chem.* **2011**, *21*, 5745−5752.

(24) Kumar, S.; Schwingenschlögl, U. Thermoelectric response of bulk and monolayer $MoSe_2$ and WSe_2. *Chem. Mater.* **2015**, *27*, 1278−1284.

(25) Kumar, N.; He, J.; He, D.; Wang, Y.; Zhao, H. Charge carrier dynamics in bulk MoS_2 crystal studied by transient absorption microscopy. *J. Appl. Phys.* **2013**, *113*, 133702.

(26) Beal, A. R.; Hughes, H. P. Kramers-Kronig analysis of the reflectivity spectra of 2H-MoS_2, 2H-$MoSe_2$ and 2H-$MoTe_2$. *J. Phys. C: Solid State Phys.* **1979**, *12*, 881.

(27) Blake, P.; Hill, E. W.; Neto, A. H. C.; Novoselov, K. S.; Jiang, D.; Yang, R.; Booth, T. J.; Geim, A. K. Making graphene visible. *Appl. Phys. Lett.* **2007**, *91*, 063124.

(28) Salehzadeh, O.; Tran, N. H.; Liu, X.; Shih, I.; Mi, Z. Exciton kinetics, quantum efficiency, and efficiency droop of monolayer MoS_2 light-emitting devices. *Nano Lett.* **2014**, *14*, 4125−4130.

(29) Brendel, M.; Kruse, A.; Jönen, H.; Hoffmann, L.; Bremers, H.; Rossow, U.; Hangleiter, A. Auger recombination in GaInN/GaN quantum well laser structures. *Appl. Phys. Lett.* **2011**, *99*, 031106.

(30) Siegner, U.; Fluck, R.; Zhang, G.; Keller, U. Ultrafast high-intensity nonlinear absorption dynamics in low-temperature grown gallium arsenide. *Appl. Phys. Lett.* **1996**, *69*, 2566−2568.

(31) Gupta, S.; Frankel, M. Y.; Valdmanis, J. A.; Whitaker, J. F.; Mourou, G. A.; Smith, F. W.; Calawa, A. R. Subpicosecond carrier lifetime in GaAs grown by molecular beam epitaxy at low temperatures. *Appl. Phys. Lett.* **1991**, *59*, 3276−3278.

(32) Kostoulas, Y.; Waxer, L. J.; Walmsley, I. A.; Wicks, G. W.; Fauchet, P. M. Femtosecond carrier dynamics in low-temperature-grown indium phosphide. *Appl. Phys. Lett.* **1995**, *66*, 1821−1823.

(33) Hong, J.; Hu, Z.; Probert, M.; Li, K.; Lv, D.; Yang, X.; Gu, L.; Mao, N.; Feng, Q.; Xie, L. Exploring atomic defects in molybdenum disulphide monolayers. *Nat. Commun.* **2015**, *6*, 6293.

(34) Chen, K.; Sheehan, N.; He, F.; Meng, X.; Mason, S. C.; Bank, S. R.; Wang, Y. Measurement of Ambipolar Diffusion Coefficient of Photoexcited Carriers with Ultrafast Reflective Grating-Imaging Technique. *ACS Photonics* **2017**, *4*, 1440−1446.

(35) Sze, S. M.; Ng, K. K. *Physics of Semiconductor Devices*, 3rd ed.; John Wiley & Sons, 2006; p 28.

(36) Su, W.; Jin, L.; Qu, X.; Huo, D.; Yang, L. Defect passivation induced strong photoluminescence enhancement of rhombic monolayer MoS_2. *Phys. Chem. Chem. Phys.* **2016**, *18*, 14001−14006.

(37) Akdim, B.; Pachter, R.; Mou, S. Theoretical analysis of the combined effects of sulfur vacancies and analyte adsorption on the electronic properties of single-layer MoS_2. *Nanotechnology* **2016**, *27*, 185701.
(38) Krivosheeva, A. V.; Shaposhnikov, V. L.; Borisenko, V. E.; Lazzari, J.-L.; Waileong, C.; Gusakova, J.; Tay, B. K. Theoretical study of defect impact on two-dimensional MoS_2. *J. Semicond.* **2015**, *36*, 122002.
(39) Valsaraj, A.; Chang, J.; Rai, A.; Register, L. F.; Banerjee, S. K. Theoretical and experimental investigation of vacancy-based doping of monolayer MoS_2 on oxide. *2D Mater.* **2015**, *2*, 045009.
(40) Chiu, M.-H.; Li, M.-Y.; Zhang, W.; Hsu, W.-T.; Chang, W.-H.; Terrones, M.; Terrones, H.; Li, L.-J. Spectroscopic signatures for interlayer coupling in MoS_2−WSe_2 van der Waals stacking. *ACS Nano* **2014**, *8*, 9649−9656.
(41) Nan, H.; Wu, Z.; Jiang, J.; Zafar, A.; You, Y.; Ni, Z. Improving the electrical performance of MoS_2 by mild oxygen plasma treatment. *J. Phys. D: Appl. Phys.* **2017**, *50*, 154001.